Separation of interference surface electromyogram into propagating and non-propagating components

Biomedical Signal Processing and Control

SEPARATION OF INTERFERENCE SURFACE ELECTROMYOGRAM INTO PROPAGATING AND NON-PROPAGATING COMPONENTS

Luca Mesin[1]

[1] *Mathematical Biology and Physiology, Dipartimento di Elettronica e Telecomunicazioni, Politecnico di Torino, Corso Duca degli Abruzzi 24, 10129, Turin, Italy*

Keywords: conduction velocity, end-of-fiber effect, interference EMG, linear electrode array

Corresponding author:

Luca Mesin, Ph.D.

Department of Electronics and Telecommunications, Politecnico di Torino, Corso Duca degli Abruzzi 24, Torino, 10129 ITALY

Tel. 0039-0110904085 Fax. 0039-0110904099 e-mail: luca.mesin@polito.it

Abstract

A new algorithm is introduced to decompose interference surface electromyogram (EMG) recorded by a multi-channel system aligned to muscle fibers into propagating and non-propagating contributions. Muscle fiber conduction velocity (CV) is also estimated, reducing the bias induced by non-propagating components. The algorithm is fast and stable, as it is based on alignment and averaging procedures. Simulated signals (with different fat thickness, SNR, number of channels, epoch duration and force level) are used to test the algorithm. The median cross-correlation of simulated and estimated components were about 98% and 90%, for propagating and non-propagating terms, respectively. CV was estimated better than using a multi-channel maximum likelihood approach applied to double differential data (mean error of 0.08 versus 0.13 m/s), with a greater gain in case of thinner fat layer, low SNR and few channels. Example applications to experimental data are also shown (single motor units action potential, M-wave and interference EMG).

Propagating components reflect the travelling of action potentials along muscle fibers. Preliminary tests show that non-propagating contributions provide selective information on motor units firing statistics. The separation of interference EMG into propagating and non-propagating components opens new perspectives, e.g., in the study of synergies, common drive and myoelectric manifestations of fatigue.

Abbreviations

CV	muscle fiber conduction velocity
DD	double differential filter
EMG	electromyogram
FD	fractal dimension
IED	inter-electrode distance
IZ	innervation zone
MU	motor unit
MUAP	motor unit action potential
MVC	maximum voluntary contraction
PSD	power spectral density
RMS	root mean square
SD	single differential filter
SFAP	single fiber action potential
SNR	signal to noise ratio

Introduction

Surface electromyogram (EMG) is the potential recorded over the skin and reflecting the distribution of current sources inducing the contraction of the muscle tissue [1-2]. Specifically, transmembrane currents are generated at the neuromuscular junctions, propagate along the muscle fibers and extinguish at the tendons. When recorded with an array of electrodes placed along the direction of muscle fibers between the innervation zone (IZ) and the tendon region, the EMG shows the propagation of the bioelectric sources, allowing to estimate their speed along the fibers, called conduction velocity (CV) [3]. CV is a physiological parameter reflecting important properties of the membrane of muscle fibers. For example, it can give indications on the peripheral condition of the neuromuscular system and its modification because of pathologies [4], fatigue [5] or exercise [6].

The definition of CV requires that the surface action potentials (AP) travel without shape distortion. This is not the case for real surface EMGs. Indeed, many factors introduce shape variations on surface APs, e.g., tissue inhomogeneity [7], additive noise [3], power line interference [1], inclination of the fibers with respect to the skin surface [8], misalignment of the fibers with respect to the detection system [9], crosstalk from nearby muscles [10-11], end-plate and end-of-fiber components [12-13]. Thus, many definitions of the delay between potentials detected from different channels can be chosen, resulting in different CV estimation methods [3].

Most perturbations to the ideal purely propagating signal derive from far field potentials that appear as non-propagating components. These contributions are mainly due to the generation of the transmembrane current at the neuromuscular junction and to its extinction at the tendon endings (end-of-fiber effect) [14], crosstalk from other muscles [10], or by the stimulation artefact in electrically elicited contractions [13]. Spatial filters have been proposed to remove common mode [15] and improve performance of algorithms applied to surface EMGs, due to their selectivity [16]. For example, double differential (DD) filter is considered in applications as the gold standard for the estimation of CV as it allows to reduce the bias of non-propagating components [17-18].

This paper addresses the problem of separating surface EMG into propagating and non-propagating components. This allows to reduce the bias on CV estimation. Moreover, the two components provide specific information (as shown in this paper), which is mixed (and more difficult to discriminate) in the original signal. Thus, it is better to estimate the non-propagating components, instead of simply removing their effect, as usually done in the literature. Two methods for the identification of non-propagating components have been proposed in the

literature [12-13]. The first method is based on an optimal choice of a pair of spatial filters that reduces the effect of non-propagating components [12]. As a by-product, the non-propagating components are also estimated, starting from the optimal filters chosen. Being based on filters with vanishing sum of weights, which have high pass behavior (reducing the SNR), the method is sensible to high frequency noise. Moreover, it is efficient in estimating non-propagating components only if they have differences in amplitudes across channels that are larger than noise. The second method is based on an adaptive filter technique (also sensitive to noise) [19] and on a computationally intensive optimization to estimate the non-propagating components [13].

Both methods can determine only one non-propagating component [12-13]. This means that only single motor units (MU) APs (MUAP) or single M-waves can be studied.

This work proposes the first method in the literature to separate propagating and non-propagating components also in interference EMGs. The method is stable, as it is based on averages (instead of differences, on which the first method was based [12]). Moreover, it requires simple and efficient operations (i.e., alignments and averaging), resulting in a low computational cost (compared to the complicated optimization procedure required by the second method [13]).

In the following sections, the method is introduced and then tested on simulated and experimental data. The performance of the method is assessed in terms of the accuracy in estimating the two components and the mean CV of active MUs (in comparison to a multi-channel approach applied to DD signals). Potential future applications are finally discussed.

Methods

A. Signal model and notations

Consider multi-channel interference surface EMGs obtained from detection points located along the direction of muscle fibers (assumed to be parallel to the skin surface). A detailed model of an interference EMG should sum the contribution of different MUAP trains, each associated to different propagating and non-propagating components. However, it is assumed here that our signal could be approximately represented using single propagating and non-propagating components. For simplicity, the model for a two-channel detection system is here discussed (but its generalization to N channels is straightforward[1]):

[1] The general expression for the kth channel is $v_k = A_k * v_p(t-(k-1)\tau) + B_k * v_{np}(t)$. Notice that IED and CV are assumed constant, so that the delays of the propagating components are multiple of a constant value τ.

$$\begin{cases} v_1(t) = A_1 * v_p(t) + B_1 * v_{np}(t) \\ v_2(t) = A_2 * v_p(t-\tau) + B_2 * v_{np}(t) \end{cases} \quad (1)$$

where $v_i(t)$ (i = 1, 2) are the recorded signals, $v_p(t)$ is the propagating component (τ being the propagation delay between channel 1 and 2) and $v_{np}(t)$ is the non-propagating one. The non-propagating component can be assumed to account for generation and extinction of transmembrane currents flowing on muscle fibers, whereas the propagating one could be ideally obtained if the muscle fibers were infinite (so that generation and extinction phenomena are removed). The two components may present different amplitudes and shape distortion, which can be described by the convolution with the functions A_i and B_i. However, clear propagating and non-propagating contributions are assumed to be present in the recorded signal, so that the convolution with the functions A_i and B_i will account only for small shape variations of the two components across channels[2].

Notice that the propagating component is assumed to have only small shape distortion across the recorded channels and its velocity of propagation is unique. As mentioned above, this assumption is critical as more MUAPs from an interference signal are considered, as in general they propagate with different CVs. This determines a distortion of the propagating component at different channels (it is worth noticing that all methods for global CV estimation from interference EMGs make implicitly the hypothesis that there is a single travelling component, even if it is constituted by the sum of MUAPs with different CVs). Moreover, this assumption requires that all MUAPs propagate in the same direction (which could be critical in the case of either pinnate muscles [20] or large spread of the IZ [18][21]).

The signals in model (1) can be either monopolar or derived by the application of a spatial filter, but monopolar detection will be assumed.

B. Estimation of the two components

The algorithm is based on the following two steps, which are iterated.

1. CV computation, alignment of signals and estimation of propagating component by averaging.

[2] Notice that there is an ambiguity in model (1), due to the multiplication between the components and the coefficients A_i and B_i. Indeed, the amplitudes of the components could be scaled by a factor, which could be compensated by a reciprocal scaling of the coefficients. However, the arbitrarity of the amplitudes of the components does not affect the algorithm, that optimally estimates the coefficients once estimated the components (see section B4).

2. Subtraction of propagating component and estimation of non-propagating component by averaging.

Notice that averaging operations are fast and stable (and useful also to remove noise). The method is further described below in details.

B.1 Estimation of the time delay of propagation

The delay was estimated by a maximum likelihood approach applied to DD data [3]. The method consists in minimizing the following mean square error function:

$$e^2(\tau) = \sum_{k=1}^{K}\sum_{n=1}^{M}\left| x_k(n) - \frac{1}{K}\sum_{m=1}^{K} x_m(n+(m-k)\tau)\right|^2 \tag{2}$$

where K is the number of DD signals (equal to N-2, where N is the number of monopolar channels) used for the estimation, M is the number of samples, $x_k(n)$ is the n^{th} sample of the k^{th} DD signal and τ is the time delay between adjacent signals to be estimated.

B.2 Estimation of the propagating component

Suppose for simplicity that the correct delay τ is known (this assumption will be dropped in section B4). Moreover, shape variations of the two components are neglected, so that the convolution operators in model (1) are substituted by scalar products (the general model, including shape variations is considered later, in Section B.5). The propagating component is estimated by aligning the signals and averaging. Considering again equation (1), including only 2 signals, we have

$$\begin{aligned}\hat{v}_p(t) &= \frac{v_1(t)+v_2(t+\tau)}{2} = \frac{A_1 v_p(t) + B_1 v_{np}(t) + A_2 v_p(t) + B_2 v_{np}(t+\tau)}{2} \\ &= \frac{A_1 + A_2}{2} v_p(t) + \frac{B_1 v_{np}(t) + B_2 v_{np}(t+\tau)}{2}\end{aligned} \tag{3}$$

If the cross-correlation of non-propagating components is small when computed for the time delay τ (which happens for example when these components are the sum of waveforms with small temporal support, as for the case of end-of-fiber components), the last term of equation (3) is reduced. Specifically, its amplitude is of the order of that of the non-propagating components divided by the number of channels used for the averaging (only 2 in equation (3), as 2 channels were considered to simplify the presentation, but more channels are used in practice). On the other hand, the first term emphasizes the propagating component, due to the constructive sum. Figure 1 shows examples of this alignment and averaging technique.

B.3 Estimation of the non-propagating component

Once estimated the propagating component, it was subtracted from the original EMGs (after optimally estimating its amplitude, as described below), obtaining the following signals y_i, i = 0, 1

$$\begin{cases} y_1(t) = v_1(t) - \hat{v}_p(t) = A_1 v_p(t) + B_1 v_{np}(t) - A_1 v_p(t) - \dfrac{2A_1}{A_1 + A_2} \dfrac{B_1 v_{np}(t) + B_2 v_{np}(t+\tau)}{2} \\ \qquad = \alpha v_{np}(t) + \beta v_{np}(t+\tau) \\ y_2(t) = v_2(t) - \hat{v}_p(t-\tau) = A_2 v_p(t-\tau) + B_2 v_{np}(t) - A_2 v_p(t-\tau) - \dfrac{2A_2}{A_1 + A_2} \dfrac{B_1 v_{np}(t-\tau) + B_2 v_{np}(t)}{2} \\ \qquad = \chi v_{np}(t) + \delta v_{np}(t-\tau) \end{cases} \quad (4)$$

where the constants α, β, χ, δ (introduced to simplify the notation) can be obtained as functions of the amplitudes A_i and B_i by collecting like terms. Notice that the propagating components were optimally subtracted (i.e., they were multiplied by the correct amplitude). The non-propagating component can now be estimated by averaging these signals

$$\hat{v}_{np}(t) = \frac{y_1(t)+y_2(t)}{2} = \frac{\alpha+\chi}{2} v_{np}(t) + \frac{\beta v_{np}(t+\tau)+\delta v_{np}(t-\tau)}{2} \quad (5)$$

The first term is the weighted average of the correct non-propagating components of each channel and is emphasized by the constructive sum, whereas the second term is the average of asynchronous contributions, which decreases in amplitude, as they are more uncorrelated. Figure 1 shows examples of this procedure to estimate non-propagating components.

B.4 Reconstruction of original data as sum of the two components and iteration

Notice that above we assumed that the delay of propagating components was known, but this is not true in general, as it can only be estimated and non-propagating components introduce a bias. However, once estimated the non-propagating component, it can be subtracted from the original signal. The resulting data have a lower content of non-propagating components, so that CV can be better estimated from them (and hence also the delay). With this improved estimation of CV, also the propagating component can be better estimated by repeating the alignment and averaging method described in Section B.2. The improved estimation of the propagating components allows to get also a better estimation of the non-propagating ones, by repeating the subtraction and averaging discussed in Section B.3. Thus, the estimation of propagating and non-propagating components can be improved by iteration. After fine-tuning on different simulations, the number of iterations was fixed equal to 30.

A crucial step in the above-mentioned algorithm is the estimation of weights of components in the original signals. Once estimated the two components, their amplitudes were optimally

computed (by pseudoinversion) in each channel (the i[th] channel is here considered), by minimizing the following functional

$$E_i = \left\| v_i(t) - A_i \hat{v}_p(t-(i-1)\tau) - B_i \hat{v}_{np}(t) \right\|_2^2 \quad (6)$$

with respect to the weights A_i and B_i.

Figure 1 shows how this iterated procedure (and the optimizations described in the following section) allows to improve the estimation of the two components.

B.5 Optimizations

Some optimizations were added to the algorithm described above. Notice that the non-propagating components are reduced by averaging after spreading them. Indeed, equations (3) and (5) show perturbations (i.e., the last terms), which are averages of delayed non-propagating components. As the algorithm is iterated, the perturbation term includes waveforms that are further delayed and reduced in amplitude. This perturbation could be reduced if the non-propagating components were subtracted before alignment of the propagating waveforms. Then, an improved estimation of the propagating component was obtained considering the following two steps. 1) After the alignment and averaging (Section B.2, equation (3)), the estimated signal was re-aligned and subtracted from each channel. 2) The samples for which this difference signal was larger than a threshold were removed and substituted by their cubic interpolation. A cleaner propagating component was then recovered again by aligning and averaging these new data. The threshold above which to select the samples to be removed was chosen by a fine-tuning on few signals: it was the standard deviation of the signal. It allowed to select only few critical points (less than 5% of the samples of the processed epoch), with a number decreasing with the iterations of the algorithm (as the non-propagating components are better removed for each iteration). Notice that this correction by interpolation is a nonlinear procedure, which removes the most important non-propagating components, reducing their spreading in the following iterations.

A second optimization consisted in allowing shape variations across channels. After estimating the components (at the end of the iterations discussed in Section B.4), possible shape variations were compensated with causal FIR filters of order 2 (equivalent results were obtained using anti-causal FIR filter of order 2). The weights of the filters were estimated by imposing optimal reconstruction of the original signals considering also delayed data, i.e., minimizing, for each channel (the i[th] is here considered), the following functional with respect to the FIR filter coefficients $A_i=[a_0, a_1, a_2]$ and $B_i=[b_0, b_1, b_2]$

$$E_i = \left\| v_i(t) - (A_i * \hat{v}_p(t-(i-1)\tau) + B_i * \hat{v}_{np}(t) \right\|_2^2 = \\ = \left\| v_i(t) - (a_0\hat{v}_p(t-(i-1)\tau) + a_1\hat{v}_p(t-(i-1)\tau-1) + a_2\hat{v}_p(t-(i-1)\tau-2) + b_0\hat{v}_{np}(t) + b_1\hat{v}_{np}(t-1) + b_2\hat{v}_{np}(t-2) \right\|_2^2 \quad (7)$$

Another optimization was applied to compute the final estimation of CV, defined as the ratio between the inter-electrode distance (IED) and the estimated time delay. After estimating the components with the method described in Sections B1-B4, the final delay and CV were close to the initial value, computed using DD signals. As the two components turned out to be estimated fairly well, an improved estimation of the delay was obtained by aligning them to the original data. Specifically, keeping fixed the estimated propagating and non-propagating components, the best delay allowing to get the minimum square error in reconstructing the original signal was computed (the quasi-Newton method was used with a cubic line search procedure and BFGS formula for updating the Hessian matrix [22]).

C. Validation of the method

The method was applied to both simulated and experimental data. Simulated signals were considered to study the effect of specific anatomies, detection or recruitment parameters. Experimental signals provided representative examples of application.

C.1 Simulated signals

A structure based, cylindrical model was used to simulate single fiber APs (SFAP), from which MUAPs were obtained. Then, the discharge pattern was generated to produce interference EMGs. The model is fully described in Appendix A and shown in Figure 2A.

Propagating and non-propagating components were computed for each SFAPs. Specifically, for each considered SFAP, another one was simulated corresponding to the same configuration, but with very long fiber, in order to estimate the propagating component only. This waveform was aligned to the SFAP corresponding to finite length fiber and windowed (Tukey window with 10% of samples used for the tapered cosine for each side) in order to remove the signal before generation and after the extinction of the current source. In this way, the propagating component was estimated for each channel. It was then subtracted from the original SFAP, obtaining the non-propagating component (reflecting the contribution due to the finite length of the fiber). The propagating and non-propagating contributions of each simulated MUAP were obtained by summing the components of the corresponding SFAPs. An example of MUAP and its components is shown in Figure 2 (B and C for 2 values of the fat layer thickness of the volume conductor, respectively).

Different simulations of interference EMGs were considered. The following parameters were used: fat layer thickness of either 3 or 7 mm; muscle force levels in the range 20-100% of the maximal voluntary contraction (MVC); epochs of 0.1-1 s duration; a number of channels in the range 4 to 7; 10 different realizations of additive white Gaussian noise band-pass filtered between 10 and 350 Hz (Chebyshev Type II filter with 20 dB attenuation in the stop-band, used in both directions to remove the phase) with signal-to-noise ratio (SNR) of 15-35 dB. The total number of simulations was 8000 (2 fat layer thicknesses × 5 force levels × 4 epoch durations × 4 arrays with different number of electrodes × 5 SNRs × 10 realizations of noise).

C.2 Measure of the performances of the method

The method was checked on simulations in terms of the accuracy of correctly estimating the two components and CV. Specifically, the cross-correlation between the estimated and simulated components was computed

$$C = \frac{\left\langle v - \mu_v, \hat{v} - \mu_{\hat{v}} \right\rangle}{\left\| v - \mu_v \right\|_2 \left\| \hat{v} - \mu_{\hat{v}} \right\|_2} \tag{8}$$

where $\langle \cdot, \cdot \rangle$ stands for scalar product, $\|\cdot\|_2$ as L_2 norm, μ_x indicates the mean value of x, v is the simulated component and $\hat{v}$ its estimation. Notice that the mean value is subtracted. However, the non-propagating component recorded between IZ and a tendon is mainly positive [23], so that the mean value of many contributions in interference EMG is positive (and highly correlated to the force level). On the other hand, the estimated propagating component has a negative mean, which is the opposite of that of the non-propagating term. In an interference signal with high force level, the mean values of the two components are lost due to phase cancellations and cannot be estimated from model (1).

In order to test the performance in estimating the time delay of propagating components, the CVs of active MUs were considered. A weighted average was computed as reference, considering the energy contribution of the MUAPs

$$CV_{REF} = \frac{\sum_{n=1}^{N_{MU}} MS_n CV_n}{\sum_{n=1}^{N_{MU}} MS_n} \tag{9}$$

where N_{MU} is the number of active MUs, MS_n is the mean square of the n^{th} MUAP and CV_n is the CV of the n^{th} MU. The rationale of this choice derives from the definition of the method used to estimate CV. It is a multi-channel CV estimation algorithm that searches the delay that guarantees the optimal alignment by minimizing the energy of the error. This means that the

estimated delay is affected by MUAPs energy. This reference value is indeed very close to the one that could be estimated by the multi-channel CV estimation algorithm if applied to a simulated interference signal obtained by summing only the propagating components of the MUAPs (as if the muscle fibers were infinite, so that the bias introduced by the non-propagating components was removed; refer to the Results section, Figure 3).

C.3 Experimental signals

Three representative examples of experimental data were considered (all data were recorded following the tenets of the Declaration of Helsinki and provided by an institution acknowledged at the end of the paper). The first two examples are the same as those considered in [13] (to which the reader is invited to refer for the details). They include single propagating and non-propagating components: the first is a single averaged MUAP obtained by decomposing monopolar EMG from the abductor pollicis brevis; the second is an M-wave recorded in single differential (SD) configuration during the transcutaneous electrical stimulation of the biceps brachii muscle. In both cases, 3 signals were considered (as the method discussed in [13] was implemented for 3 channels only). Thus, 2 double differentiations could not be computed: then, CV was estimated considering the 3 available signals (notice that 2 DD data could be obtained from the 3 M-waves in SD configuration, but they could not be obtained from the 3 monopolar signals from the abductor pollicis; thus, CV was computed in both cases using the 3 available channels).

The last signal is an interference EMG recorded during a free voluntary contraction of the biceps brachii using a linear array of 32 electrodes with IED of 5 mm (from which 8 channels showing unidirectional propagation were selected). Signals were detected in monopolar derivation (referred to a remote reference on the wrist), amplified (183 V/V), band-pass filtered (3 dB bandwidth, 10–500 Hz), sampled at 2048 Hz and A/D converted with 16 bits resolution (multi-channel surface EMG amplifier, LISiN, Politecnico di Torino, Italy [24]).

Results

Figure 3 shows an example of application to simulated data. Propagating and non-propagating components were estimated and compared to the simulated ones in Figure 3A. Notice in Figure 3B that the power spectral densities (PSD) of the two components (and mainly of the non-propagating one) emphasize a low frequency peak (which is present, but small on the original

data) located at the average firing frequency of MUs. Different force levels were also considered in Figure 3C. The reference CV, defined in equation (8), is very similar to the one that could be estimated using the simulated propagating component. Accurate estimations are obtained also using the proposed method, whereas a small underestimation was found using DD signals.

Figure 4 shows the distributions of the correlation between the estimated and simulated components, grouping the data in order to show the dependence on specific parameters. Better estimations of propagating and non-propagating components were obtained for thinner and thicker fat layers, respectively, i.e., in the case in which they are more evident (statistically significant differences, Wilkoxon rank sum test with $p<0.01$).

Figure 5 shows the distribution of errors in estimating CV. In the average, they were lower for the new method, than for the standard one (even if the difference was not statistically significant; however, significant differences were obtained in the specific cases indicated in the figure). A volume conductor with a thick fat layer was considered, which is the worst case: when considering a thinner fat layer, propagating components were estimated better (as stated before, discussing Figure 4) and, as a consequence, also CV estimation was more accurate (and statistically better than that obtained using DD signals; Wilkoxon rank sum test with $p<0.01$).

Figure 6 shows representative applications to experimental data. Only qualitative comments can be given, as there is no a-priori information on the two components and propagation velocity. However, reasonable results are obtained. Indeed, the non-propagating terms estimated from the single MUAP in Figure 6A include generation and end-of-fiber components. Moreover, when processing the M-wave shown in Figure 6B, the stimulation artefact is identified as the main non-propagating term. Notice also another contribution at the end of the wave, which is a residual of extinction effect still present in the considered SD signals. Larger non-propagating components can be seen in monopolar M-waves and found interesting applications in the recent literature [25]. It is worth noticing also that the estimated propagating component is less noisy than the raw data (beneficial effect of the averaging).

The interference signal shown in Figure 6C was split into components that are clearly propagating and non-propagating. Looking at the raw data, the separation appears to be reasonable and qualitatively similar to the one obtained in simulations (refer to Figure 3A).

The method was implemented and run in Matlab, using a PC with Intel(R) Core i7-7500U CPU, Double-Core (but only one core was used), clock frequency 2.7 GHz, 8 GB of RAM and 64 bits operating system. It required in the average 450 and 720 ms to process epochs of duration

500 and 1000 ms, respectively, thus allowing in principle real time applications in which data are acquired and transferred in epochs that are processed while waiting for subsequent samples.

Discussion

Surface EMG recorded over muscles with fibers parallel to the skin from linear arrays of electrodes placed between the IZ and a tendon can be approximately split into propagating and non-propagating contributions. The first reflects the travelling of APs along muscle fibers and the second is related to their generation and extinction (or to common mode interference). Both components provide important information, so that their separation could open new perspectives in the study of surface EMG, with potential outcomes in basic physiology and applications. A few previous results were discussed in the literature [12-13][19], showing the possibility of applying such a separation to improve CV estimation [12], identify the stimulation artefact and measure automatically the fiber semi-length [13]. However, these methods were quite unstable and computationally intensive. Furthermore, they were limited to process single contributions (i.e., single MUAPs or M-waves). Probably, this important drawback limited their diffusion in applications.

This paper describes a stable and efficient method, which is the first in the literature to separate interference EMG into propagating and non-propagating components. Stability and efficiency were improved with respect to previous methods, as the new algorithm is only based on alignments and averaging procedures (which are fast and stable). Indeed, preliminary tests on the single MUAP shown in Figure 6A corrupted with different levels of white Gaussian noise showed greater correlation of the two components with the ones obtained from the original data and lower variation of the estimated CV, when using the new algorithm. Moreover, the mean time to process a MUAP with the two methods [12-13] was more than 10 times larger than that taken by the new algorithm.

However, the most important improvement is the extension of the range of applications to interference data. Interference EMG is very reach: Appendix B shows that each time sample may reflect the superposition of tens of MUAPs. The asynchronous summation of such MUAPs reflects into phase cancellations [26], which largely reduce the information content of the signal. However, the proposed algorithm showed in simulations to be able to split the original EMG into components that are highly correlated to the correct ones. Indeed, median correlations were about 98% and 90%, for propagating and non-propagating components, respectively.

CV estimations were always better than those obtained using the standard multi-channel method based on DD signals, when a volume conductor with thin fat layer was considered (as in that case the propagating component was estimated fairly well, with a median correlation with the simulated component of 98.7%). In Figures 4 and 5, the results are shown for a volume conductor with large fat thickness, which is the worst case. However, the new method still outperforms the standard one in the average. Moreover, being based on alignments and averages, the method attenuates random noise. This allowed to get better estimations of CV than the standard approach in the case of small SNRs. The accuracy was not affected by the simulated force level. However, notice that a constant SNR was simulated, whereas in experimental signals a larger SNR is expected to be found for increasing force. The method was also stable to the shortening of the epochs. Moreover, CV estimations were more accurate than those provided by the standard method when the number of electrodes decreased (the improvement was statistically significant with less than 6 electrodes).

The method showed to have good convergence in separating the two components under physiological conditions. It can fail if the propagating component is too fast, as it is more difficult to separate it from the non-propagating one. Indeed, the alignment-averaging procedure (described in the Methods sections B2 and B3) assumes that the alignment of one component implies the misalignment of the other. If the propagating component is too fast, its alignment does not allow to misalign enough the non-propagating one to reduce its effect by averaging. Thus, the performances of the method are expected to decrease by increasing the average MU CV. Preliminary tests on simulations were run by rescaling MUAPs to simulate a distribution of MU CV which had mean value ranging from 1.5 to 20 m/s (using the same distribution described in the Methods section, but translating all MU CVs by a constant to center it around the new mean value). Simulation parameters were the followings: 4 electrodes, IED of 5 mm, force level 50% MVC, SNR of 25 dB, epoch duration of 1 s, fat layer thickness of either 3 or 7 mm. The estimated and simulated propagating and non-propagating components had high correlation coefficients (greater than 95 and 80% for the two components, respectively) from low values of average CV until 10 m/s (which is higher than physiological values), above which the correlation rapidly dropped. A similar problem could be experienced if IED is too small (e.g., lower than 2 mm, so that the average delay of MUAPs considering mean MU CV of 4 m/s will be the same as the one obtained considering IED of 5 mm and mean CV of 10 m/s).

The new method is stable to possible detection problems. A misalignment of 20° between the array of electrodes and the muscle fibers was simulated, considering all cases already studied

in the ideal conditions. The median correlations between estimations and simulations were about 95% and 78%, for propagating and non-propagating components, respectively. The mean error in CV estimation were 0.13 and 0.29 m/s, considering the new and the standard methods, respectively (statistically highly significant difference for Wilkoxon rank sum test). Notice however that there are many important conditions in which the method cannot be applied, as the assumption that the EMG is the sum of two components is not a reliable approximation. For example, it cannot be applied in the case of muscles with fibers going deep [8] or when there are multiple directions of propagation (as in the case of distributed IZs [18], pinnate muscles [20] or in the external anal sphincter [21]).

Many additional applications of the method can be addressed in the future, apart from the possibility of improving CV estimation. For example, non-propagating components are far-field potentials providing information also on activity of deep MUs, thus collecting data from a large portion of the muscle. Moreover, their contributions are shorter (mainly corresponding to end-of-fiber components) than those of travelling APs. Thus, they convey information with higher longitudinal selectivity (i.e., in time [15]), allowing to better separate different contributions, than using propagating components. This property may help when studying inter-muscle coherence and phase synchronization [27].

The separation of the two components could also be useful to quantify crosstalk from nearby muscles. A preliminary test was done on a few simulated signals used for a recent study on crosstalk [11] (volume conductor with fat thickness of 7 mm). Two superficial and adjacent muscles were activated at 80% and 40% MVC, respectively, and EMGs were recorded over the two muscles, at 20 mm from the midline separating them. The discharge patterns of their MUs were independent, but cross-correlation and phase synchronization of signals recorded over the two muscles were about 60% and 48%, respectively, due to crosstalk. When considering the propagating component, cross-correlation and phase synchronization decreased to 42% and 34%, whereas they increased to 74% and 61% when using the non-propagating components. Indeed, the propagating components are near-field potentials, providing information on the muscle under the electrodes, whereas non-propagating components reflect far-field potentials coming from both muscles. Thus, a combination of information derived from the two components could be useful to discern crosstalk and co-activation of nearby muscles.

Non-propagating components are also expected to reflect the overall discharge rate of active MUs, as they are built–up by sharp contributions due to generation and extinction phenomena. This hypothesis was tested on a few simulated data from [5] (the first simulated library was considered). EMGs reflecting different adjustments of MU behavior during fatiguing

contractions were simulated in [5]. Variations of mean CVs, maximal firing rate, MU synchronization and variability of inter-spike interval were considered. Fractal dimension (FD) of EMG was found to be mostly related to central fatigue and only marginally affected by different mean CVs [5]. When estimated on non-propagating components, FD was still less affected by CV (as it mostly affects propagating components). Moreover, the PSD of non-propagating components was about bimodal (whereas the PSD of original signals was unimodal). The low frequency peak was related to the firing statistics [28]: its amplitude increased with larger synchronism among MUs and its location reflected the mean firing rate (as also found in the specific example shown in Figure 3). The relation between the average MU firing rate and the PSD of the estimated non-propagating components in the low frequency range was recently assessed extensively in simulations [29]. A low frequency peak reflecting the average firing rate was found in the estimated non-propagating components also for high contraction levels, whereas it didn't emerge when using the raw EMG (either rectified or not). Thus, the separation of the raw EMG into propagating and non-propagating components could help deepening the study of myoelectric fatigue, by better distinguishing among different manifestations (either peripheral or central, reflecting either firing rate modulation or MU synchronization).

These are only preliminary examples of applications on crosstalk, phase synchronization, fatigue and MU firing rate, which, together with the reduction of bias in CV estimation, indicate that the separation of the two components in interference signal may have potential relevance that future investigation can assess.

Conclusions

This paper introduces a stable and efficient method to separate multi-channel interference surface EMG into propagating and non-propagating components. The two components provide different important information: propagating components reflect the travelling of APs along muscle fibers; non-propagating components are related to generation and extinction of APs and provide selective information on the MU firing statistics. This separation opens new perspectives in the study of surface EMG, with many possible applications, e.g., in the study of synergies, common drive and myoelectric manifestations of fatigue.

Appendix

A. Simulation model. The simulation model was the same as in [11] (to which the reader can refer for details). Specifically, a cylindrical model was used to simulate SFAPs [30]. The

volume conductor and simulated muscle are indicated in Figure 2. The following parameters were assumed: skin conductivity $2.2 \cdot 10^{-2}$ S/m; fat conductivity $4 \cdot 10^{-2}$ S/m; transversal and longitudinal conductivity of muscle tissue $9 \cdot 10^{-2}$ and $40 \cdot 10^{-2}$ S/m, respectively. Seven square electrodes (surface 1 mm^2) with inter-electrode distance of 5 mm were placed over the skin, aligned to the fibers (Figure 2). Monopolar SFAPs were simulated for fibers with length and location of IZ randomly chosen with a range of variation of 10 mm, as indicated in 2A. Simulated density of muscle fibers was $20/mm^2$. It is about the fiber density of a MU, an order of magnitude lower than that of a muscle [31]. The same fibers were included in different MUs with superimposed territory, introducing an approximation. The number of fibers per MU was distributed exponentially between 15 and 300. The total number of simulated MUs was 400. Their locations were randomly chosen within the muscle with uniform distribution. The fibers closest to the center of a MU were selected to belong to it and the corresponding SFAPs were added up to simulate the MUAP. CV of MUs was chosen with a Gaussian distribution with mean 4 m/s and standard deviation 0.3 m/s. CV values were assigned in agreement to the size principle.

Interference signals were simulated as in [31], with range of recruitment thresholds equal to 70% of MVC, range of the firing rate (FR) 8-30 Hz (with linear increase with the force level with slope of 1 Hz per 1% MVC, after MU recruitment and until the upper limit of the FR) and 10% random (Gaussian) jitter of the inter-spike interval.

B. Estimation of MUAP number in interference EMG. Consider a contraction at an average force intensity, e.g., 50% MVC. Assume that 100 MUs are active and within the detection volume of the considered monopolar channels and that they are firing at an average frequency of 30 Hz. Those MUs fire 3000 times per s, which is about 4 times the sampling frequency required by Nyquist theory (considering for EMG a bandwidth of about 350-400 Hz). Moreover, each MUAP can have a duration of more than 15 ms (considering fiber length of 60 mm, CV of 4 m/s and including the time needed for extinction of the AP). Thus, in this condition, each time sample of EMG in the average shows the asynchronous superposition of about 50 MUAPs.

Conflict of interest

The author has no potential conflicts of interest to be disclosed.

Acknowledgments: Experimental data were recorded following the Declaration of Helsinki and provided by LISiN (Laboratorio di Ingegneria del Sistema Neuromuscolare e della riabilitazione motoria, Turin, Italy).

References

[1] R. Merletti, M. Aventaggiato, A. Botter, A. Holobar, H. Marateb, T. M. Vieira, Advances in surface EMG: recent progress in detection and processing techniques. Crit. Rev. Biomed. Eng. 38(4) (2010) 305-45.

[2] L. Mesin, Volume conductor models in surface electromyography: Computational techniques. Comput. Biol. Med. 43(7) (2013) 942-52.

[3] D. Farina, R. Merletti, Methods for estimating muscle fiber conduction velocity from surface electromyographic signals. Med. Biol. Eng. Comput. 42(4) (2004) 432-45.

[4] M. J. Zwarts, G. Drost, D. F. Stegeman, Recent progress in the diagnostic use of surface EMG for neurological diseases. J. Electromyogr. Kinesiol. 10(5) (2000) 287-91. Review.

[5] L. Mesin, D. Dardanello, A. Rainoldi, G. Boccia, Motor unit firing rates and synchronisation affect the fractal dimension of simulated surface electromyogram during isometric/isotonic contraction of vastus lateralis muscle. Med. Eng. Phys. 38(12) (2016) 1530-33.

[6] G. A. Rongen, J. P. van Dijk, E. E. van Ginneken, D. F. Stegeman, P. Smits, M. J. Zwarts, Repeated ischaemic isometric exercise increases muscle fiber conduction velocity in humans: involvement of Na(+)-K(+)-ATPase. J. Physiol. 540 (Pt 3) (2002) 1071-8.

[7] L. Mesin, Simulation of Surface EMG Signals for a Multi-layer Volume Conductor with Triangular Model of the Muscle Tissue. IEEE Trans. Biomed. Eng. 53(11) (2006) 2177-84.

[8] L. Mesin, R. Merletti, T. M. Vieira, Insights gained into the interpretation of surface electromyograms from the gastrocnemius muscles: A simulation study. J. Biomech. 44(6) (2011) 1096-103.

[9] D. Farina, C. Cescon, R. Merletti, Influence of anatomical, physical and detection-system parameters on surface EMG. Biol. Cybern. 86(6) (2002) 445–56.

[10] N. A. Dimitrova, G. V. Dimitrov, O. A. Nikitin, Neither high-pass filtering nor mathematical differentiation of the EMG signals can considerably reduce cross-talk. J. Electromyogr. Kinesiol. 12(4) (2002) 235-46.

[11] L. Mesin, Optimal spatio-temporal filter for the reduction of crosstalk in surface electromyogram. J. Neural. Eng., 15(1) (2018) 016013.

[12] L. Mesin, F. Tizzani, D. Farina. Estimation of motor unit conduction velocity from surface EMG recordings by signal-based selection of the spatial filters. IEEE Trans. Biomed. Eng. 53(10) (2006) 1963-71.

[13] L. Mesin, A. K. R. Kandoor, R. Merletti. Separation of propagating and non-propagating components in surface EMG. Biomed. Sig. Proc. Contr. 3(2) (2008) 126-37.

[14] N. A. Dimitrova, G. V. Dimitrov, Z. C. Lateva, Influence of the fiber length on the power spectra of single muscle fiber extracellular potentials. Electromyogr. Clin. Neurophysiol. 31(6) (1991) 387-98.

[15] D. Farina, L. Mesin, S. Martina, R. Merletti, Comparison of spatial filter selectivity in surface myoelectric signal detection: influence of the volume conductor model. Med. Biol. Eng. Comput. 42(1) (2004) 114-20.

[16] H. Huang, P. Zhou, G. Li, T. Kuiken, Spatial filtering improves EMG classification accuracy following targeted muscle reinnervation. Ann Biomed Eng. 37(9) (2009) 1849-57.

[17] H. Broman, G. Bilotto, C. J. De Luca, A note on non invasive estimation of muscle fiber conduction velocity. IEEE Trans. Biomed. Eng. 32(5) (1985) 341-3.

[18] M. Nielsen, T. Graven-Nielsen, D. Farina, Effect of innervation-zone distribution on estimates of average muscle-fiber conduction velocity. Muscle Nerve 37(1) (2008) 68-78.

[19] J. Rubio Vela, R. Merletti, Y. Fan, Separation of travelling from non-travelling components in surface myoelectric signals. Proceedings of the VI Mediterranean Conference on Medical and Biological Engineering, Capri, Italy, vol. I, July 5-10, 1992.

[20] L. Mesin, L. Damiano, D. Farina. Estimation of average muscle fiber conduction velocity from simulated surface EMG in pinnate muscles. J. Neurosci. Methods. 160 (2007) 327–34.

[21] Enck P, Franz H, Davico E, Mastrangelo F, Mesin L, Merletti R. Repeatability of innervation zone identification in the external anal sphincter muscle. Neurourol Urodyn. 29(3) (2010) 449-57.

[22] R. Fletcher, Practical Methods of Optimization. vol. 1, Unconstrained Optimization, John Wiley and Sons, 1980.

[23] L. Mesin, Estimation of monopolar signals from sphincter muscles and removal of common mode interference. Biomed. Sig. Proc. Contr. 4(1) (2009) 37-48.

[24] G. L. Cerone, A. Botter, M. Gazzoni, A Modular, Smart, and Wearable System for High Density sEMG Detection. Submitted to IEEE Trans. Biomed. Eng. 2018.

[25] J. Rodriguez-Falces, N. Place. End-of-fiber signals strongly influence the first and second Phases of the M-Wave in the vastus lateralis: Implications for the Study of Muscle Excitability. Front. Physiol. 9(162) (2018).

[26] K. G. Keenan, D. Farina, R. Merletti, R. M. Enoka, Amplitude cancellation reduces the size of motor unit potentials averaged from the surface EMG. J. Appl. Physiol. 100(6) (2006) 1928-37.

[27] L. Wang, A. Lu, S. Zhang, W. Niu, F. Zheng, M. Gong, Fatigue-related electromyographic coherence and phase synchronization analysis between antagonistic elbow muscles. Exp. Brain. Res. 233(3) (2015) 971-82.

[28] J. Basmajian, C. J. De Luca, Muscles Alive: Their function revealed by electromyography, 5th ed., Williams and Wilkins, Baltimore, 1985.

[29] L. Mesin, Non-propagating components of surface electromyogram reflect motor unit firing rates. Medical Engineering & Physics (submitted), 2019.

[30] D. Farina, L. Mesin, S. Martina, R. Merletti, A surface EMG generation model with multilayer cylindrical description of the volume conductor. IEEE Trans Biomed Eng. 51(3) (2004) 415-26.

[31] J. Fuglevand, D. A. Winter, A. E. Patla, Models of recruitment and rate coding organization in motor-unit pools. J. Neurophysiol. 70(6) (1993) 2470-88.

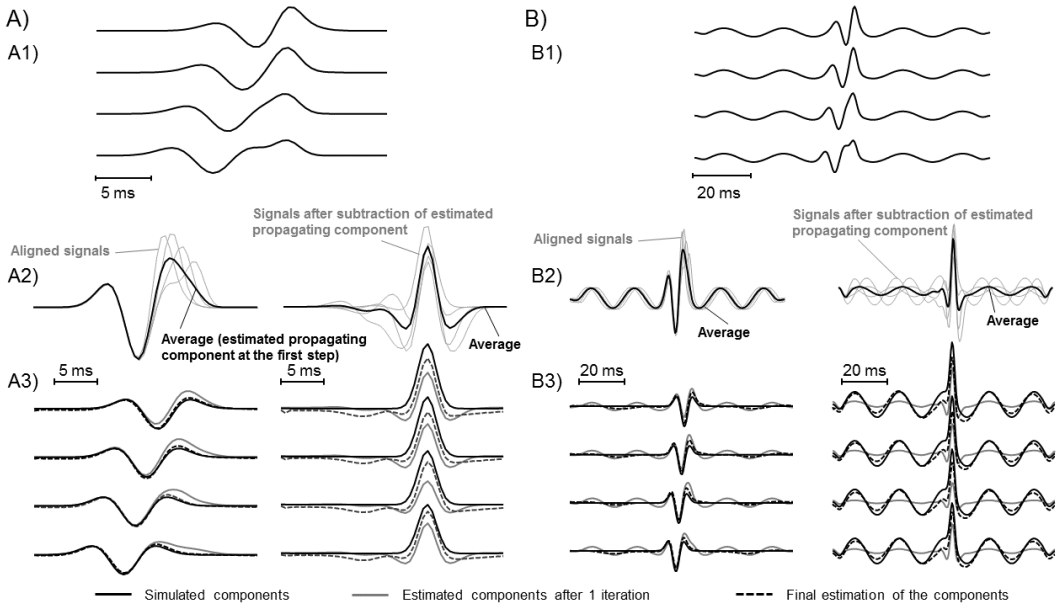

Figure 1. Examples of separation of the two components. A) Propagating component is a doubly differentiated Gaussian function, the non-propagating one is a Gaussian function with different amplitude across channels. A1) Input data, A2) averaging process to get the first estimation of the components, A3) the two components estimated after the first step (reconstruction RMS errors 44% and 61%, for propagating and non-propagating components, respectively) and at the end (errors 17% and 24%). B) Same as in A), but adding a 50 Hz interference (reconstruction errors 102% and 78% after one step, 49% and 39% at the end of iterations).

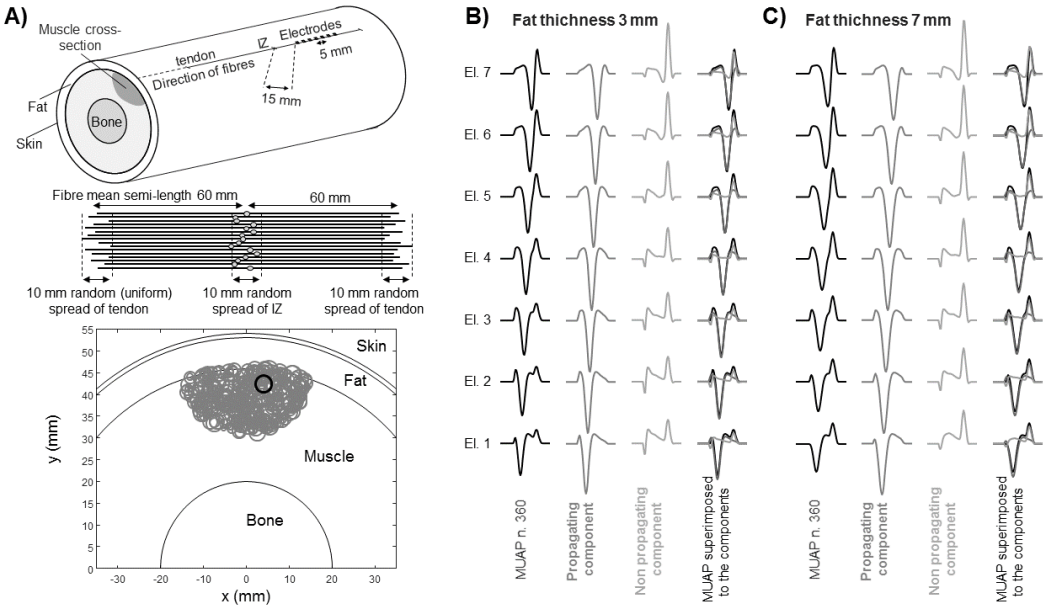

Figure 2. A) Volume conductor model used for the simulations (3D representation with the location of the 7 electrodes, longitudinal section showing the spread of the IZ and tendon endings, cross-section with indication of center and cross-sectional area of MUs; the black circle indicates MU number 360). B)-C) Examples of a MUAP (of MU number 360) and separation into two components for a volume conductor with a fat thickness of either 3 or 7 mm (B and C, respectively).

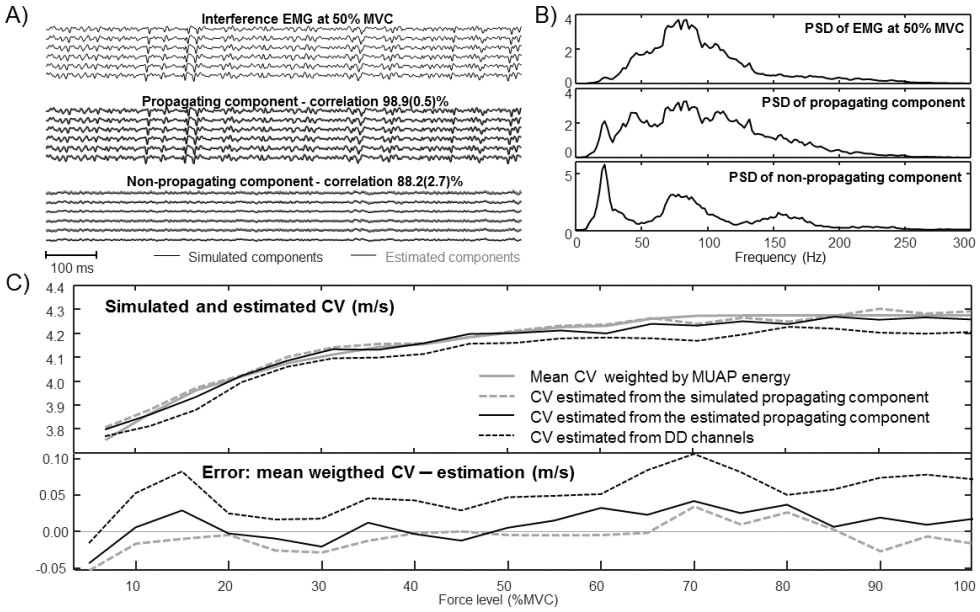

Figure 3. Example of simulated monopolar interference EMG (sampling frequency 2048 Hz, fat layer thickness of 3 mm, SNR = 20 dB). A) Simulated data and estimated components over time (mean and standard deviation of correlation across channels indicated). B) Power spectral density (PSD) of data and components (fourth channel; Welch method, averaging estimates from 7 sub-epochs of 250 ms, superimposed of 50%). C) Comparison of reference CV (weighted by energy of MUAPs of active MUs) and the estimation using either simulated or estimated propagating components or the standard multi-channel approach applied to DD signals (estimations and errors in the upper and lower panels, respectively).

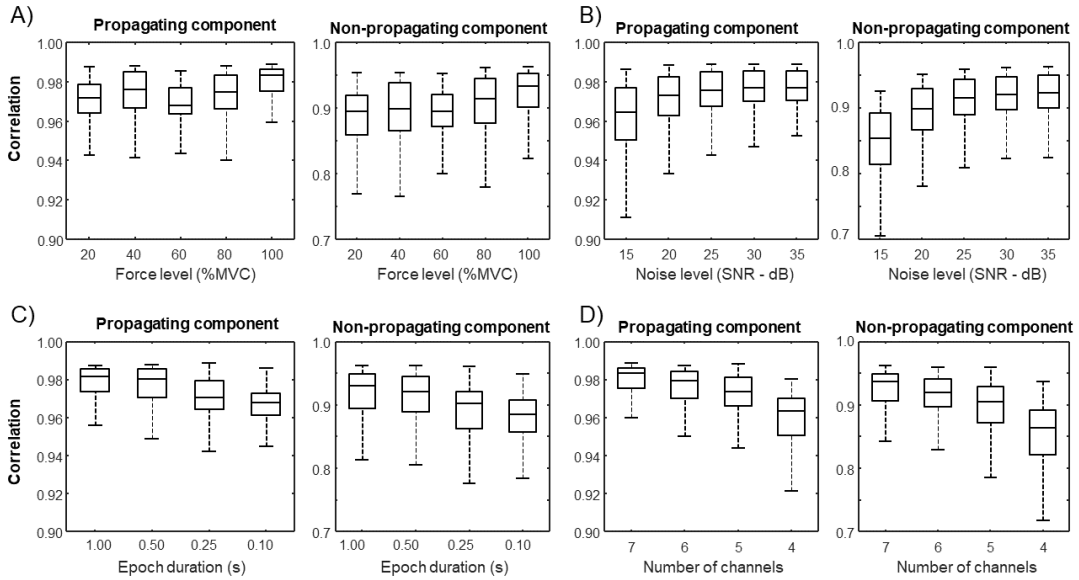

Figure 4. Cross-correlation of estimated and simulated propagating and non-propagating components, grouping data with respect to A) force, B) noise level, C) epoch duration and D) number of channels. The fat layer thickness was 7 mm. With a thickness of 3 mm, propagating component was estimated better and non-propagating components worst (median values 98.7% and 86.4% versus 97.4% and 90.6%, for propagating and non-propagating components, respectively; statistical significance tested by Wilkoxon rank sum test with p=0.01).

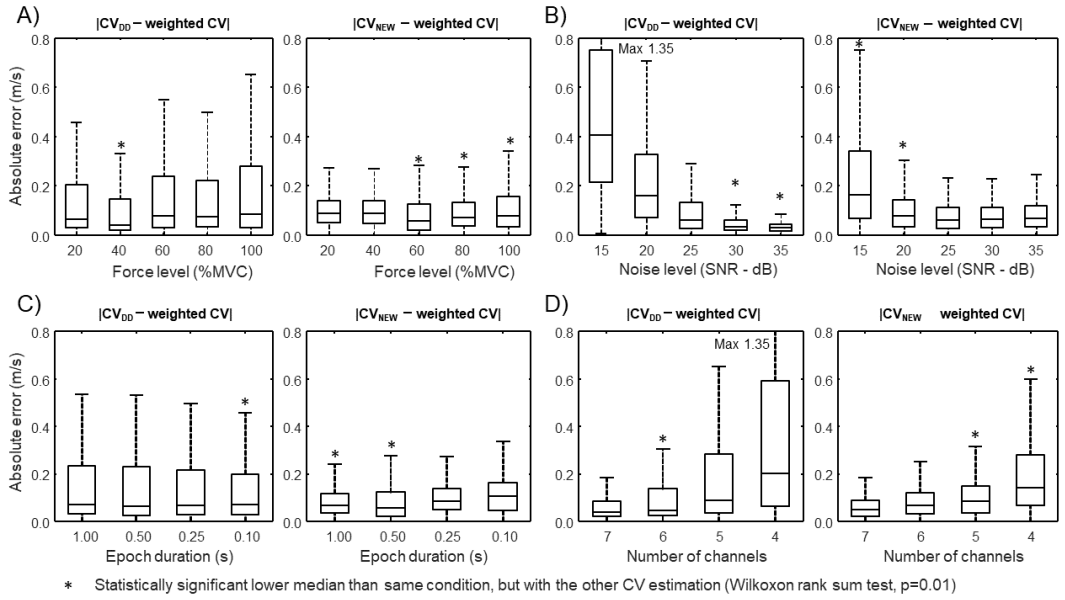

Figure 5. Absolute error in estimating average CV weighted by MUAP energy, grouping data with respect to A) force, B) noise level, C) epoch duration and D) number of channels. The fat layer thickness was 7 mm. With a thickness of 3 mm, the median errors were always lower when considering the new method and the difference statistically significant (Wilkoxon rank sum test, p=0.01), with the only exception of the case of epoch duration 0.1 s.

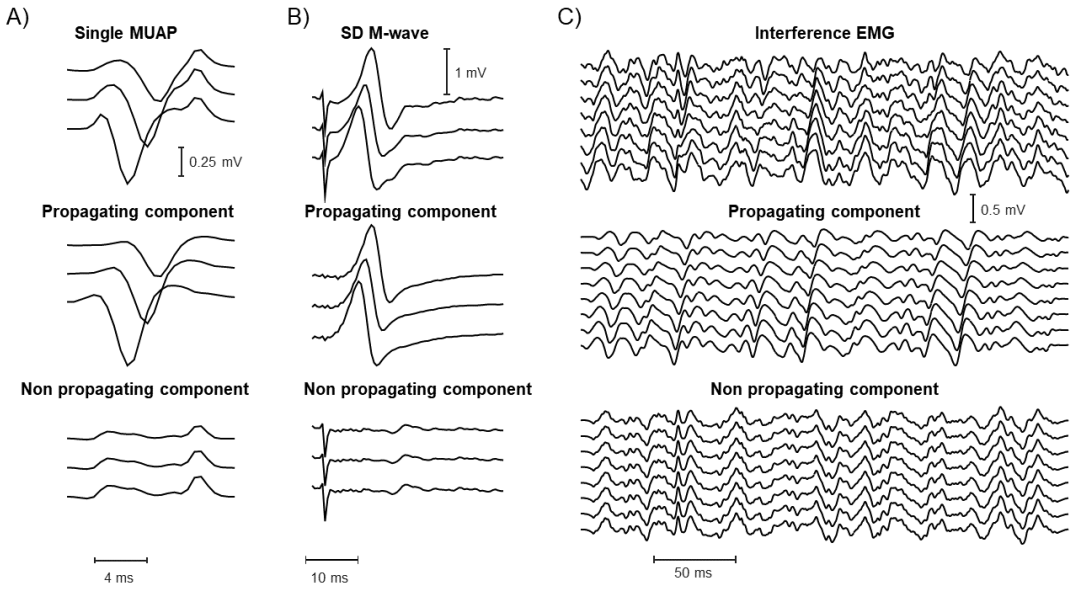

Figure 6. Examples of applications to experimental data. A) Single MUAP extracted from the abductor pollicis brevis (monopolar configuration). B) M-wave induced by the transcutaneous electrical stimulation of the biceps brachii (single differential signals). C) Interference EMG during voluntary contraction of the biceps brachii. Eight signals showing propagation of action potentials were selected out of 32 monopolar EMGs recorded by a linear array aligned to the muscle fibers (and showing bi-directional propagation from the IZ region towards proximal and distal tendons; the distal portion was selected).